

Air Force Institute of Technology

AFIT Scholar

Faculty Publications

2019

Ir⁴⁺ Ions in β -Ga₂O₃ Crystals: An Unintentional Deep Donor

Christopher A. Lenyk

Nancy C. Giles

Air Force Institute of Technology

Elizabeth M. Scherrer

Brant E. Kananen

Larry E. Halliburton

West Virginia University

See next page for additional authors

Follow this and additional works at: <https://scholar.afit.edu/facpub>



Part of the [Atomic, Molecular and Optical Physics Commons](#), and the [Semiconductor and Optical Materials Commons](#)

Recommended Citation

C.A. Lenyk, N.C. Giles, E.M. Scherrer, B.E. Kananen, L.E. Halliburton, K.T. Stevens, G.K. Foundos, J.D. Blevins, D.L. Dorsey, and S. Mou, *J. Appl. Phys.* 125, 045703 (2019). <https://doi.org/10.1063/1.5081825>

This Article is brought to you for free and open access by AFIT Scholar. It has been accepted for inclusion in Faculty Publications by an authorized administrator of AFIT Scholar. For more information, please contact richard.mansfield@afit.edu.

Authors

Christopher A. Lenyk, Nancy C. Giles, Elizabeth M. Scherrer, Brant E. Kananen, Larry E. Halliburton, K. T. Stevens, G. K. Foundos, James D. Blevins, D. L. Dorsey, and S. Mou

Ir^{4+} ions in $\beta\text{-Ga}_2\text{O}_3$ crystals: An unintentional deep donor

C. A. Lenyk,¹ N. C. Giles,^{1,a)} E. M. Scherrer,¹ B. E. Kananen,¹ L. E. Halliburton,² K. T. Stevens,³
G. K. Foundos,³ J. D. Blevins,⁴ D. L. Dorsey,⁵ and S. Mou⁵

¹*Department of Engineering Physics, Air Force Institute of Technology, Wright-Patterson Air Force Base, Ohio 45433, USA*

²*Department of Physics and Astronomy, West Virginia University, Morgantown, West Virginia 26506, USA*

³*Northrop Grumman Synoptics, 1201 Continental Blvd., Charlotte, North Carolina 28273, USA*

⁴*Air Force Research Laboratory, Sensors Directorate, Wright Patterson Air Force Base, Ohio 45433, USA*

⁵*Air Force Research Laboratory, Materials and Manufacturing Directorate, Wright-Patterson Air Force Base, Ohio 45433, USA*

Abstract

Electron paramagnetic resonance (EPR) and infrared absorption are used to detect Ir^{4+} ions in $\beta\text{-Ga}_2\text{O}_3$ crystals. Mg and Fe doped crystals are investigated and concentrations of Ir^{4+} ions greater than $1 \times 10^{18} \text{ cm}^{-3}$ are observed. The source of the unintentional deep iridium donors is the crucible used to grow the crystal. In the Mg-doped crystals, the Ir^{4+} ions provide compensation for the singly ionized Mg acceptors, and thus contribute to the difficulties in producing *p*-type behavior. The Ir^{4+} ions replace Ga^{3+} ions at the Ga(2) sites, with the six oxygen neighbors forming a distorted octahedron. A large spin-orbit coupling causes these Ir^{4+} ions to have a low-spin ($5d^5$, $S = 1/2$) ground state. The EPR spectrum consists of one broad line with a significant angular dependence. Principal values of the *g* matrix are 2.662, 1.815, and 0.541 (with principal axes near the crystal *a*, *b*, and *c* directions, respectively). Ionizing radiation at 77 K decreases the Ir^{4+} EPR signal in Mg-doped crystals and increases the signal in Fe-doped crystals. In addition to the EPR spectrum, the Ir^{4+} ions have an infrared absorption band representing a *d-d* transition within the t_{2g} orbitals. At room temperature, this band peaks near 5153 cm^{-1} ($1.94 \mu\text{m}$) and has a width of 17 cm^{-1} . The band is highly polarized: its intensity is a maximum when the electric field *E* is parallel to the *b* direction in the crystal and is nearly zero when *E* is along the *c* direction.

^{a)}Author to whom correspondence should be addressed: Nancy.Giles@afit.edu

INTRODUCTION

Ritter *et al.*¹ have recently reported the presence of Ir⁴⁺ ions in β -Ga₂O₃ crystals doped with Mg acceptors. In the present paper, electron paramagnetic resonance (EPR) and infrared absorption are used to further characterize this important impurity in Mg and Fe doped crystals.²⁻⁹ The iridium ions are an unintentional deep donor in bulk β -Ga₂O₃ crystals grown with iridium crucibles, by either the Czochralski method or the edge-defined film-fed growth method.¹⁰⁻¹² In *n*-type crystals, the iridium is present as Ir³⁺ ions. In crystals with a lower Fermi level (e.g., Mg or Fe doped), a portion of the iridium will also be present as Ir⁴⁺ ions. In semiconductor terms, the Ir³⁺ and Ir⁴⁺ ions are neutral donors (D⁰) and singly ionized donors (D⁺), respectively. Based on the similar radii of Ga³⁺, Ir³⁺, and Ir⁴⁺ ions in sixfold coordinated sites,¹³ the iridium ions in β -Ga₂O₃ crystals are expected to be located at the octahedral Ga(2) positions. The Ga(2) location of the Ir ions is also supported by computational studies.¹

The Ir⁴⁺ ions are unique and especially interesting in β -Ga₂O₃. They have the [Xe]4f¹⁴5d⁵ configuration. In their distorted octahedral environment, a large spin-orbit coupling and a strong crystal field cause the Ir⁴⁺ ions to have a low-spin (S = 1/2) ground state, as the five *d* electrons are placed in the three *t*_{2g} orbitals ($\uparrow\downarrow\uparrow$).¹⁴ This gives rise to an anisotropic EPR signal and also produces an infrared absorption signal when an electron is promoted from one orbital to another within the three *t*_{2g} orbitals. In contrast, the Ir³⁺ (5d⁶) ions have no EPR signal as there are three sets of paired *d* electrons in the *t*_{2g} orbitals. In the early years of paramagnetic resonance, EPR spectra from Ir⁴⁺ ions played an important role when the conceptual understanding of low-spin *d*⁵ octahedral complexes and the sharing of spin density (i.e., covalency) with neighboring ions was being developed.¹⁵⁻¹⁸ Recently, the study of Ir⁴⁺ ions in iridate compounds such as Sr₂IrO₄ have revealed new and unusual properties of matter caused by the combined effects of strong spin-orbit and Coulomb interactions.¹⁹⁻²²

Iridium is a significant donor in β -Ga₂O₃ crystals grown in iridium crucibles, as this impurity provides a deep level that affects the electrical and optical properties of the material. In the present paper, we investigate the EPR and infrared absorption properties of Ir⁴⁺ ions in this wide-

band-gap semiconductor. The complete angular dependence of the $S = 1/2$ EPR spectrum is acquired, thus establishing the principal values and principal directions of the g matrix. The temperature dependence and polarization properties of the 5153 cm^{-1} infrared absorption band are also determined. Correlations of the intensities of the EPR spectrum and the infrared absorption band in both Mg and Fe doped samples verify that these spectral features have a common origin. Combining the EPR and infrared results allows an oscillator strength to be estimated for the absorption band. A change in the concentration of Ir^{4+} ions occurs when a crystal is exposed to above-band-gap photons (i.e., ionizing radiation) while at or near 77 K. X rays are used in this study for convenience, but near-band-edge light from a lamp or a laser is expected to be equally effective. The ionizing radiation at 77 K causes the Ir^{4+} EPR signal to decrease in Mg-doped crystals and to increase in Fe-doped crystals. Subsequent warming to near or slightly above room temperature, respectively, restores the pre-irradiated intensities.

II. EXPERIMENTAL

The bulk $\beta\text{-Ga}_2\text{O}_3$ crystals used in the present investigation were grown by the Czochralski technique with iridium crucibles. Crystals doped with Mg were obtained from Synoptics (a Northrop Grumman company in Charlotte, NC). The starting material contained approximately 0.20 mol.% of MgO. Crystals doped with Fe were provided by Kyma Technologies (Raleigh, NC) and had 0.01 mol.% of Fe_2O_3 added to the starting materials. The samples were rectangular b plates, approximately $3 \times 4 \text{ mm}^2$ with thickness ranging from 0.36 to 1.4 mm. EPR and infrared absorption spectra were obtained from four samples (two Mg-doped and two Fe-doped), thus allowing a correlation study. An EPR spectrum from Fe^{3+} ions is present in all the samples, very intense in the Fe-doped samples and smaller, yet easily detected, in the Mg-doped samples. The a , b , and c crystal directions for each sample were verified using the angular dependence of the Fe^{3+} EPR spectrum.²³ Errors in aligning the crystals in our experiments were less than 5° .

A Bruker EMX spectrometer operating near 9.39 GHz was used to take the EPR spectra. Magnetic fields were measured with a Bruker NMR teslameter and the temperature of the sample

was controlled with an Oxford helium-gas flow system. Estimates of the concentration of defects contributing to an EPR spectrum, valid to within a factor of two, were based on comparisons to a standard pitch sample provided by Bruker. A Varian OEG-76H-Rh tube operating at 60 kV and 30 mA was used for the x-ray irradiations. Infrared absorption spectra were taken with a ThermoScientific Nicolet 8700 FTIR spectrometer. A white-light (QTH) source, a CaF₂ beam splitter, and a DTGS detector were used, along with an ultra-broad-band (250 nm to 4 μm) fused-silica wire-grid polarizer from Thorlabs (Model WP25M-UB). A liquid-nitrogen cryostat with sapphire windows from Cryo Industries (Model 110-637-DED) and a LakeShore (Model 335) controller were used to take the low-temperature infrared absorption data. Effects of surface losses have been removed from the absorption spectra shown in this paper.

III. EPR RESULTS

Figure 1 shows the EPR spectrum obtained at 30 K from an Mg-doped β-Ga₂O₃ crystal. The magnetic field is along the *b* direction in the crystal and the microwave frequency is 9.393 GHz. Five intense lines are observed. The broad line at 369.9 mT is assigned to Ir⁴⁺ ions, while lines at 165.7, 305.1, 607.1, and 1341.8 mT are due to Fe³⁺ ions. Neutral Mg acceptors (Mg_{Ga}⁰) are not present in the spectrum in Fig. 1, as these acceptors⁸ are all compensated and thus in their singly ionized charge state (Mg_{Ga}⁻). Large zero-field splittings, comparable in energy to our 9.39 GHz microwave photons, are responsible for the complex Fe³⁺ spectrum.²³ These Fe³⁺ (3*d*⁵) ions have the high-spin *S* = 5/2 ground state, with the B₂ and B₄ coefficients for the Stevens operators in the monoclinic spin Hamiltonian having large values. This causes multiple Fe³⁺ lines, as the distinction between allowed and forbidden transitions is no longer valid. Also, significant shifts in the positions of lines occur when the direction of the magnetic field is changed. In contrast, the Ir⁴⁺ (5*d*⁵) ions have the low-spin *S* = 1/2 ground state. As seen in Fig. 1, the EPR spectrum of the Ir⁴⁺ ions in β-Ga₂O₃ crystals is much simpler with only an *M*_s = +1/2 to -1/2 transition. The concentration of ions responsible for the Ir⁴⁺ EPR signal in Fig. 1 is estimated to be approximately 7.0 × 10¹⁸ cm⁻³. [Note that the linewidth of the Ir⁴⁺ signal is about 12.0 mT, whereas the linewidths

of the Fe^{3+} signals are about 1.5 mT.] Above 115 K, the Ir^{4+} EPR signal broadens because of a short spin-lattice relaxation time. Below 20 K, a long spin-lattice relaxation time causes the Ir^{4+} line to show signs of saturation with increasing microwave power. During our study, we did not observe an EPR spectrum that could be assigned to Ir^{2+} ($5d^7$) ions. Spectra from Ir^{2+} ions, however, have been reported in other materials.^{24,25}

Figure 2 shows the angular dependence of our Ir^{4+} EPR spectrum. The position of the line was measured at 5° intervals as the direction of the magnetic field was rotated in the a - b , b - c , and c - a^* planes, where the b direction is normal to the mirror plane. Because a and c are 103.8° apart in these crystals,^{26,27} a^* and c^* directions are introduced (a^* is perpendicular to b and c whereas c^* is perpendicular to a and b).²⁸ The space group for monoclinic β - Ga_2O_3 is $C2/m$, thus allowing for two distinct, crystallographically equivalent, orientations of the principal axes of the g matrix for point defects located at sixfold Ga(2) sites. There are two cases to be considered, since these two orientations of the g matrix may or may not be magnetically equivalent. In the first case, where the principal axes of the g matrix are along arbitrary directions, the two orientations of the g matrix will be magnetically equivalent when the magnetic field is aligned along the a , b , or c directions and at all angles in the a - c plane (i.e., the mirror plane) and will not be magnetically equivalent when rotating in the a - b and b - c planes. This results in a single line in the a - c plane and two distinct lines in the a - b and b - c planes. Site splitting of this type in a monoclinic material has been seen in the angular dependence of Sb^{2+} ($5s^25p^1$) impurity ions at Sn sites in photorefractive $\text{Sn}_2\text{P}_2\text{S}_6$ crystals.²⁹ In the second case, where the principal axes of the g matrix are along the a , b , and c directions, the two orientations of the g matrix are always magnetically equivalent and a single line will be observed in all three planes of rotation. Our experimental results in Fig. 2, with no detectable splittings in the a - b and b - c planes, correspond to this second case, thus indicating that the principal-axis directions of the g matrix for the Ir^{4+} ions must be near the crystal's a , b , and c directions.

As illustrated by the angular dependence in Fig. 2, the Ir^{4+} ions have a highly anisotropic g matrix. The EPR line moves from a low magnetic field of 253 mT to a high field of 1235 mT

during the rotations. Turning points near a and c identify two of the principal-axis directions of the g matrix, with the third principal axis along the b direction (i.e., perpendicular to the mirror plane). A spin Hamiltonian with an electron Zeeman term ($H = \beta \vec{S} \cdot \vec{g} \cdot \vec{B}$) describes the angular dependence and allows the four parameters that define the g matrix to be determined. In the a,b,c^* coordinate system, these parameters are the three diagonal elements and one off-diagonal element. The 45 discrete points in Fig. 2, along with their corresponding microwave frequencies, were used as input data for a “least-squares” fitting procedure. The energy eigenvalues of the 2×2 spin Hamiltonian matrix were repeatedly calculated as the g -matrix parameters were systematically varied during the fitting process. Best-fit values for the four parameters are given in Table I. Final principal g values and principal-axis directions (X,Y,Z) were obtained when the upper matrix in Table I was diagonalized. The solid curves in Fig. 2 were generated using these final parameters. Our g values for the Ir^{4+} ions in $\beta\text{-Ga}_2\text{O}_3$ crystals are similar to those reported for Ir^{4+} ions in TiO_2 (see Table I).³⁰

The average of our three principal g values for Ir^{4+} in $\beta\text{-Ga}_2\text{O}_3$ is 1.673. Sharing of the Ir^{4+} d electrons with the six neighboring oxygen ions (and also with the Ga ions beyond these six oxygen ions) is responsible for this averaged g value being considerably less than the free spin value of 2.0023.¹⁴⁻¹⁸ If an Ir^{4+} ion is located at the center of a perfect (i.e., cubic) octahedron, the g matrix will be isotropic. The observed anisotropy in the g matrix with large shifts of the three principal values from the averaged value indicates that, as expected, the oxygen octahedron surrounding the Ir^{4+} ion is significantly distorted in the monoclinic $\beta\text{-Ga}_2\text{O}_3$ crystal. The following equations describe the g values of an Ir^{4+} ion in a low symmetry site.^{14,17,31,32}

$$g_z = \cos^2 \theta \left\{ g_e \sin^2 \alpha - (g_e + 2k) \cos^2 \alpha \right\} + (2k - g_e) \sin^2 \theta \quad (1)$$

$$\frac{1}{2}(g_x + g_y) = -\cos^2 \theta \left\{ g_e \sin^2 \alpha + 2\sqrt{2}k \cos \alpha \sin \alpha \right\} \quad (2)$$

$$\frac{1}{2}(g_x - g_y) = \sin 2\theta \left\{ g_e \cos \alpha + \sqrt{2}k \sin \alpha \right\} \quad (3)$$

$$\tan(2\alpha) = \frac{2\sqrt{2}\lambda}{\lambda - 2\Delta} \quad (4)$$

In Eqs. (1-3), k is the orbital reduction factor (an indicator of covalency) and α and θ describe the linear combination of d orbitals that form the ground state doublet of the Ir^{4+} ion. In Eq. (4), λ is the spin-orbit coupling constant and Δ is the infrared absorption energy. As discussed in Ref. 17, there are two choices for the relative signs of g_x , g_y , and g_z . [Note that these signs are not experimentally determined.] We find that the following relative signs ($g_x = -2.662$, $g_y = -1.815$, and $g_z = +0.541$) give realistic values for the three Ir^{4+} parameters k , α , and θ in $\beta\text{-Ga}_2\text{O}_3$. Our best-fit results using Eqs. (1-3) are:

$$k = 0.646, \quad \alpha = 58.5^\circ, \quad \theta = -6.7^\circ.$$

The small value for k reinforces our expectation that there is significant sharing of the d electrons with the six neighboring oxygen ions. Equation (4) provides a connection between the EPR spectrum and the infrared absorption peak position and allows us to determine a value for λ . Using $\alpha = 58.5^\circ$ and $\Delta = 5153 \text{ cm}^{-1}$ from Section IV gives $\lambda = 4215 \text{ cm}^{-1}$. This value for λ is within the range of 3000 to 4500 cm^{-1} often invoked for Ir^{4+} ions.^{30,33,34}

Many of the EPR spectra reported for Ir^{4+} ions in various materials have resolved hyperfine structure from the ^{191}Ir and ^{193}Ir nuclei.³⁵⁻³⁸ These isotopes have $I = 3/2$ nuclear spins and similar nuclear magnetic moments.³⁹ Their natural abundances are 37.3% and 62.7%, respectively. In all reported cases, the hyperfine matrices are nearly isotropic, with principal values (in energy units) near $25 \times 10^{-4} \text{ cm}^{-1}$. The EPR line in Fig. 1 from the Ir^{4+} ions is very broad, approximately 12.5 mT, with no resolved hyperfine structure from ^{191}Ir and ^{193}Ir nuclei. This lack of resolved hyperfine lines in the $\beta\text{-Ga}_2\text{O}_3$ Ir^{4+} spectrum is not surprising. In addition to a broadening of the four expected lines as a result of superhyperfine interactions with the nearest $^{69,71}\text{Ga}$ nuclei, the nuclear electric quadrupole interactions for the $^{191,193}\text{Ir}$ nuclei must also be considered. Large nuclear electric quadrupole moments for the $^{191,193}\text{Ir}$ nuclei³⁹ and a large electric field gradient at the Ga(2) sites in this low-symmetry crystal will cause the Ir^{4+} ions in $\beta\text{-Ga}_2\text{O}_3$ to have a complex hyperfine pattern consisting of strongly overlapping allowed and forbidden lines. This, together with the Ga superhyperfine interactions, produce the observed broad almost structureless EPR line. We attribute the very slight distortion at the mid-point of the Ir^{4+} EPR line, when the mag-

netic field is along the b direction, to underlying nuclear electric quadrupole effects (see Figs 6 and 7). The EPR spectra from Ir^{4+} ions in MgO and CaO crystals have been fully analyzed and the results of large nuclear quadrupole interactions have been clearly illustrated.³⁵ We anticipate that future electron-nuclear double resonance (ENDOR) experiments will provide similar complete sets of $^{191,193}\text{Ir}$ hyperfine parameters for Ir^{4+} ions in $\beta\text{-Ga}_2\text{O}_3$ crystals.

IV. INFRARED ABSORPTION RESULTS

Figure 3 shows the infrared absorption spectrum from Ir^{4+} ions in an Mg-doped $\beta\text{-Ga}_2\text{O}_3$ crystal. This infrared band, first observed by Ritter *et al.*,¹ is a $d-d$ transition within the t_{2g} orbitals of the low-spin Ir^{4+} ions. Similar sharp absorption bands in the 4500 to 5300 cm^{-1} region have been reported in the past for Ir^{4+} ions in various host crystals.^{30,33,36,40,41} As illustrated in Fig. 3, the width and thus the intensity of this band in $\beta\text{-Ga}_2\text{O}_3$ is strongly temperature dependent. At room temperature, the band peaks at 5153 cm^{-1} (1.94 μm) and its full-width-at-half-maximum (FWHM) is 17 cm^{-1} . The band sharpens as the temperature is lowered. At 80 K, the peak shifts to 5148.1 cm^{-1} and the FWHM reduces to 1.2 cm^{-1} . In Fig. 3, the right vertical scale goes with the room temperature spectrum and the left vertical scale goes with the 80 K spectrum. The Ir^{4+} absorption band in Fig. 3 has a Lorentzian shape and represents a weakly allowed electronic transition. Vibronic structure near the main peak was not observed.

Figure 4 shows that the 5153 cm^{-1} infrared absorption band is polarized. The maximum intensity occurs when the electric field vector E of the incident light is parallel to the b direction in the crystal. With the electric field E near c^* , the intensity of this absorption band decreases to near zero. Figure 5 shows the change in the intensity of the infrared absorption band as the direction of the electric field is varied from a to c^* . The solid curve in Fig. 5 is generated using $I(\theta) = A + B\cos^2\theta$ for the intensity (i.e., the transition probability) of the absorption band,⁴² where $\theta = 0^\circ$ when E is along a and $\theta = 90^\circ$ when E is along c^* .

A primary result of the present study is the correlation of the intensities of the EPR signal and the infrared absorption peak for Ir^{4+} ions in $\beta\text{-Ga}_2\text{O}_3$. Data were obtained from four crystals.

Two are Mg-doped (labeled Mg1 and Mg2) and two are Fe-doped (labeled Fe1 and Fe2). The results are presented in Table II. The third column is the room-temperature absorption coefficient α for the 5153 cm^{-1} infrared band. These values were acquired with light propagating along the b direction and the electric field E along the a direction. The fourth column is the concentration N of Ir^{4+} ions obtained from EPR spectra taken at 40 K with the magnetic field along the b direction. Larger values of α and N are expected for the Mg-doped crystals since a greater portion of the iridium ions are in the 4+ charge state when Mg acceptors are present. In the fifth column of Table II, the ratios of N and α for the four crystals are used to determine if a correlation exists. As can be seen, this ratio is very nearly the same for the four samples, thus providing evidence that the infrared absorption band and the EPR line are from the same defect. The deviations from the average value of $2.4 \times 10^{18} \text{ cm}^{-2}$ for the N/α values in Table II are less than 9%. In future investigations, if one of the two quantities N or α is known, then the other can be estimated using the equation $N = [2.4 \times 10^{18} \text{ cm}^{-2}]\alpha$.

Combining EPR and optical absorption data from the same crystal allows us to determine an oscillator strength f for the Ir^{4+} infrared absorption band. The EPR spectrum in Fig. 1 and the room-temperature absorption spectrum in Fig. 4 were taken from the same Mg-doped crystal (referred to as crystal Mg1 in Table II). Smakula's equation, given in Eq. (5) for a Lorentzian line shape, relates the product of defect concentration N and oscillator strength f to the intensity and FWHM of the absorption band and the index of refraction n of the material.^{43,44}

$$Nf = (1.29 \times 10^{17}) \frac{n}{(n^2 + 2)^2} \alpha_{\max} W \quad (5)$$

The concentration N of Ir^{4+} ions from the EPR spectrum in Fig. 1 is $7.0 \times 10^{18} \text{ cm}^{-3}$, and α_{\max} and W from the maximum absorption data in Fig. 4, taken with the electric field along the b direction, are 6.2 cm^{-1} and 2.2 meV , respectively. Near the $1.9 \text{ }\mu\text{m}$ position of the peak, the index of refraction n of $\beta\text{-Ga}_2\text{O}_3$ is 1.9.⁴⁵ Substituting these quantities into Eq. (5) gives an oscillator strength $f = 1.5 \times 10^{-5}$ for the Ir^{4+} infrared absorption band in $\beta\text{-Ga}_2\text{O}_3$. If the refractive index and local field correction factors are ignored, f becomes 2.5×10^{-4} . These results for f are consistent with

expected values of oscillator strengths for $d-d$ transitions.⁴⁶

V. EFFECTS OF ABOVE-BAND-GAP PHOTONS

Ionizing radiation (i.e., above-band-gap photons) was found to change the concentration of Ir^{4+} ions in the Mg-doped and Fe-doped $\beta\text{-Ga}_2\text{O}_3$ crystals. We used x rays, but near-band-edge light from a lamp or a laser is also expected to produce similar effects. In our experiments, the above-band-gap photons form “free” electrons and holes. At 77 K, the majority of these electrons and holes immediately recombine, but some become trapped at existing deep donors and acceptors. These electrons and holes remain trapped for long periods of time when the crystal is kept at a sufficiently low temperature.

Figure 6 shows the effects of a 77 K x -ray irradiation on an Mg-doped $\beta\text{-Ga}_2\text{O}_3$ crystal. These spectra were taken at 40 K with the magnetic field along the b direction. In Fig. 6(a), the spectrum taken before the exposure to x rays shows EPR signals from Fe^{3+} and Ir^{4+} ions, but not from Mg acceptors. The Mg acceptors are not present in Fig. 6(a) because they are all in their singly ionized nonparamagnetic charge state (Mg_{Ga}^-), compensated in large part by the Ir^{4+} ions. This is consistent with the large concentration of Ir^{4+} ions observed in Fig. 1 and listed in Table II. After the irradiation at 77 K with x rays, the Mg-doped crystal was cooled to 40 K, with no intervening warming, and the EPR spectrum in Fig. 6(b) was taken. The characteristic spectrum⁸ from the neutral Mg acceptors (Mg_{Ga}^0) is now present and the intensities of the Fe^{3+} and Ir^{4+} signals have both decreased by 41% from their pre-irradiated values. The following is a possible explanation for these observations. During the 77 K irradiation of the Mg-doped crystal, the Fe^{3+} and Ir^{4+} ions trap electrons and become Fe^{2+} and Ir^{3+} ions while, at the same time, the singly ionized Mg acceptors (Mg_{Ga}^-) trap holes and become neutral acceptors (Mg_{Ga}^0).

The effects of x rays are quite different for the Fe-doped $\beta\text{-Ga}_2\text{O}_3$ crystals. EPR spectra were taken at 40 K from an Fe-doped crystal before and after an irradiation at 77 K with x rays. These results are shown in Fig. 7. Because of the large difference in the intensities of the Fe^{3+} and Ir^{4+} signals (due to the high level of Fe doping), the before and after Fe^{3+} spectra were taken

with one set of spectrometer conditions and the before and after Ir⁴⁺ spectra were taken with a different set of spectrometer conditions. For the Ir⁴⁺ spectra, higher microwave power and a larger modulation amplitude were used. After the irradiation, the intensity of the Fe³⁺ EPR signal is reduced by a factor of 1.7 (i.e., the signal is 40% less than its pre-irradiated value) whereas the Ir⁴⁺ EPR signal is a factor of 3.2 larger than its pre-irradiated value. This decrease of the Fe³⁺ signal and increase of the Ir⁴⁺ signal is consistent with the Fe ions being acceptors^{4,6,7} and the Ir ions being donors. Specifically, Fe³⁺ ions trap electrons during the irradiation and become Fe²⁺ ions while nonparamagnetic Ir³⁺ ions trap holes and become Ir⁴⁺ ions. The Fe³⁺ and Ir⁴⁺ ions slowly revert to their pre-irradiation concentrations when the crystal is returned to room temperature. This recovery was 60% complete after the crystal was held for five min at room temperature.

VI. SUMMARY

Large crystals of β -Ga₂O₃ are often grown by the Czochralski or edge-defined film-fed methods using iridium crucibles, and thus contain significant concentrations of isolated iridium ions. These unintentional deep donors are present as Ir³⁺ ($5d^6$) ions in *n*-type crystals. When the Fermi level is lower, Ir⁴⁺ ($5d^5$) ions will also be present. We use EPR and infrared absorption to observe these Ir⁴⁺ ions in Mg and Fe doped crystals. The Ir⁴⁺ ions occupy Ga(2) sites with the six oxygen neighbors forming a distorted octahedron. Because of a large spin-orbit interaction, these $5d^5$ ions have a low-spin $S = 1/2$ ground state. Principal *g* values of the resulting anisotropic EPR spectrum are 2.662, 1.815, and 0.541. Also, the Ir⁴⁺ ions have a room-temperature infrared absorption band peaking at 5153 cm⁻¹. This *d-d* band has a small oscillator strength and is highly polarized. In the Mg-doped crystals, the Ir⁴⁺ ions are the primary source of compensation for the Mg acceptors. The presence of the iridium ions is expected to make *p*-type doping of bulk-grown crystals more difficult. Of special interest are the photon-induced changes in the charge state of the iridium donors. During an exposure at 77 K to ionizing radiation (*x* rays in our experiments), the concentration of Ir⁴⁺ ions decreased in Mg-doped crystals and increased in Fe-doped crystals. These results suggest that the Fe impurities behave as acceptors and prefer to be in the Fe³⁺ or

Fe^{2+} states and the Ir impurities behave as donors and prefer to be in the Ir^{4+} or Ir^{3+} states.

ACKNOWLEDGMENTS

The present work was supported in part by the Air Force Office of Scientific Research under award numbers F4FGA08054J003 and FA9550-18RYCOR098. Any opinions, findings, and conclusions or recommendations expressed in this paper are those of the authors and do not necessarily reflect the views of the United States Air Force.

ACCEPTED MANUSCRIPT

References

- ¹J. R. Ritter, J. Huso, P. T. Dickens, J. B. Varley, K. G. Lynn, and M. D. McCluskey, “Compensation and hydrogen passivation of magnesium acceptors in β -Ga₂O₃,” Appl. Phys. Lett. **113**, 052101 (2018).
- ²S. J. Pearton, J. Yang, P. H. Cary, F. Ren, J. Kim, M. J. Tadjer, and M. A. Mastro, “A review of Ga₂O₃ materials, processing, and devices,” Appl. Phys. Rev. **5**, 011301 (2018).
- ³M. H. Wong, C.-H. Lin, A. Kuramata, S. Yamakoshi, H. Murakami, Y. Kumagai, and M. Higashiwaki, “Acceptor doping of β -Ga₂O₃ by Mg and N ion implantations,” Appl. Phys. Lett. **113**, 102103 (2018).
- ⁴A. T. Neal, S. Mou, S. Rafique, H. Zhao, E. Ahmadi, J. S. Speck, K. T. Stevens, J. D. Blevins, D. B. Thomson, N. Moser, K. D. Chabak, and G. H. Jessen, “Donors and deep acceptors in β -Ga₂O₃,” Appl. Phys. Lett. **113**, 062101 (2018).
- ⁵J. L. Lyons, “A survey of acceptor dopants for β -Ga₂O₃,” Semicond. Sci. Technol. **33**, 05LT02 (2018).
- ⁶A. Y. Polyakov, N. B. Smirnov, I. V. Shchemerov, S. J. Pearton, Fan Ren, A. V. Chernykh, and A. I. Kochkova, “Electrical properties of bulk semi-insulating β -Ga₂O₃ (Fe),” Appl. Phys. Lett. **113**, 142102 (2018).
- ⁷M. E. Ingebrigtsen, J. B. Varley, A. Yu. Kuznetsov, B. G. Svensson, G. Alfieri, A. Mihaila, U. Badstübner, and L. Vines, “Iron and intrinsic deep level states in Ga₂O₃,” Appl. Phys. Lett. **112**, 042104 (2018).
- ⁸B. E. Kananen, L. E. Halliburton, E. M. Scherrer, K. T. Stevens, G. K. Foundos, K. B. Chang, and N. C. Giles, “Electron paramagnetic resonance study of neutral Mg acceptors in β -Ga₂O₃ crystals,” Appl. Phys. Lett. **111**, 072102 (2017).
- ⁹Q. D. Ho, T. Frauenheim, and P. Deák, “Theoretical confirmation of the polaron model for the Mg acceptor in β -Ga₂O₃,” J. Appl. Phys. **124**, 145702 (2018).
- ¹⁰M. Baldini, Z. Galazka, and G. Wagner, “Recent progress in the growth of β -Ga₂O₃ for power electronics applications,” Mater. Sci., Semicond. Process. **78**, 132 (2018).

- ¹¹A. Kuramata, K. Koshi, S. Watanabe, Y. Yamaoka, T. Masui, and S. Yamakoshi, “High-quality β -Ga₂O₃ single crystals grown by edge-defined film-fed growth,” *Jpn. J. Appl. Phys.* **55**, 1202A2 (2016)
- ¹²L. Pidol, O. Guillot-Noël, M. Jourdir, A. Kahn-Harari, B. Ferrand, P. Dorenbos, and D. Gourier, “Scintillation quenching by Ir³⁺ impurity in cerium doped lutetium pyrosilicate crystals,” *J. Phys.: Condens. Matter* **15**, 7815 (2003).
- ¹³R. D. Shannon, “Revised effective ionic radii and systematic studies of interatomic distances in halides and chalcogenides,” *Acta Cryst. A* **32**, 751 (1976).
- ¹⁴A. Abragam and B. Bleaney, “Electron Paramagnetic Resonance of Transition Ions,” (Oxford University Press, London, 1970) Chapter 8.
- ¹⁵J. H. E. Griffiths, J. Owen, and I. M. Ward, “Paramagnetic resonance in palladium and platinum group compounds,” *Proc. Roy. Soc. A* **219**, 526 (1953).
- ¹⁶J. H. E. Griffiths and J. Owen, “Complex hyperfine structures in microwave spectra of covalent iridium compounds,” *Proc. Roy. Soc. A* **226**, 96 (1954).
- ¹⁷B. Bleaney and M. C. M. O’Brien, “Paramagnetic resonance in some complex cyanides of the iron group II. Theory,” *Proc. Phys. Soc. B* **69** 1216 (1956).
- ¹⁸J. H. M. Thornley, The magnetic properties of (IrX₆)²⁻ complexes,” *J. Phys. C: Solid State Phys.* **1**, 1024 (1968).
- ¹⁹N. A. Bogdanov, V. M. Katukuri, J. Romhányi, V. Yushankhai, V. Kataev, B. Büchner, J. van den Brink, and L. Hozoi, “Orbital reconstruction in nonpolar tetravalent transition-metal oxide layers,” *Nat. Commun.* **6**, 7306 (2015).
- ²⁰K. S. Pedersen et al., “Iridates from the molecular side,” *Nat. Commun.* **7**, 12195 (2016).
- ²¹G. Cao and P. Schlottmann, “The challenge of spin-orbit-tuned ground states in iridates: a key issues review,” *Rep. Prog. Phys.* **81**, 042502 (2018).
- ²²S. Fuchs, T. Dey, G. Aslan-Cansever, A. Maljuk, S. Wurmehl, B. Büchner, and V. Kataev, “Unraveling the nature of magnetism of the 5d⁴ double perovskite Ba₂YIrO₆,” *Phys. Rev. Lett.* **120**, 237204 (2018).

- ²³M. L. Meil'man, "EPR of Fe³⁺ ions in β -Ga₂O₃ crystals," Sov. Phys. Solid State **11**, 1403 (1969).
- ²⁴A. Raizman, J. T. Suss, and W. Low, "Quadrupole interaction and static Jahn-Teller effect in the EPR spectra of Ir²⁺ in MgO and CaO," Phys. Rev. B **15**, 5184 (1977).
- ²⁵J. M. Gaité and H. Rager, "Electron paramagnetic resonance study of iridium in forsterite," Phys. Chem. Minerals **30**, 628 (2003).
- ²⁶S. Geller, "Crystal structure of β -Ga₂O₃," J. Chem. Phys. **33**, 676 (1960).
- ²⁷J. Åhman, G. Svensson, and J. Albertsson, "A reinvestigation of β -gallium oxide," Acta Cryst. **C52**, 1336 (1996).
- ²⁸T. H. Yeom, I. G. Kim, S. H. Lee, S. H. Choh, and Y. M. Yu, "Electron paramagnetic resonance characterization of Cr³⁺ impurities in a β -Ga₂O₃ single crystal," J. Appl. Phys. **93**, 3315 (2003).
- ²⁹A. T. Brant, L. E. Halliburton, S. A. Basun, A. A. Grabar, S. G. Odoulov, A. Shumelyuk, N. C. Giles, and D. R. Evans, "Photoinduced EPR study of Sb²⁺ ions in photorefractive Sn₂P₂S₆ crystals," Phys. Rev. B **86**, 134109 (2012).
- ³⁰K. W. Blazey and F. Levy, "EPR of rhodium, osmium and iridium-doped rutile," Solid State Commun. **59**, 335 (1986).
- ³¹X. F. Hu, S. Y. Wu, G. L. Li, Y. Q. Xu, C. C. Ding, and Z. H. Zhang, "Studies of the local lattice distortions for the various rhombic Ru³⁺ centres in AgX (X = Cl and Br)," Polyhedron **117**, 14 (2016).
- ³²L. L. Li, S. Y. Wu, P. Xu, and S. X. Zhang, "Studies on the spin Hamiltonian parameters and local structure for Rh⁴⁺ and Ir⁴⁺ in TiO₂," Phys. Chem. Minerals **37**, 497 (2010).
- ³³B. Andlauer, J. Schneider, and W. Tolksdorf, "Optical absorption, fluorescence, and electron spin resonance of Ir⁴⁺ on octahedral sites in Y₃Ga₅O₁₂," Phys. Stat. Sol. B **78**, 533 (1976).
- ³⁴J. P. Clancy, N. Chen, C. Y. Kim, W. F. Chen, K. W. Plumb, B. C. Jeon, T. W. Noh, and Y.-J. Kim, "Spin-orbit coupling in iridium-based 5d compounds probed by x-ray absorption spectroscopy," Phys. Rev. B **86**, 195131 (2012).

- ³⁵A. Raizman and J. T. Suss, “Electron paramagnetic resonance of Ir⁴⁺ ions in MgO and CaO,” *Phys. Rev. B* **22**, 1141 (1980).
- ³⁶O. F. Schirmer, A. Forster, H. Hesse, M. Wohlecke, and S. Kapphan, “Paramagnetic resonance and near-infrared optical absorption of SrTiO₃: Ir⁴⁺,” *J. Phys. C: Solid State Phys.* **17**, 1321 (1984).
- ³⁷E. Possenriede, O. F. Schirmer, H. J. Donnerberg, and B. Hellermann, “ESR investigation of transition metal defects in KNbO₃,” *J. Phys.: Condens. Matter* **1**, 7267 (1989).
- ³⁸E. Possenriede, P. Jacobs, and O. F. Schirmer, “Paramagnetic defects in BaTiO₃ and their role in light-induced charge transport: I. ESR studies,” *J. Phys.: Condens. Matter* **4**, 4719 (1992).
- ³⁹N. J. Stone, “Table of nuclear magnetic dipole and electric quadrupole moments,” *At. Data Nucl. Data Tables* **90**, 75 (2005).
- ⁴⁰T. A. Keiderling, P. J. Stephens, S. B. Piepho, J. L. Slater, and P. N. Schatz, “Infrared absorption and magnetic circular dichroism of Cs₂ZrCl₆:Ir⁴⁺,” *Chem. Phys.* **11**, 343 (1975).
- ⁴¹G. C. Allen, R. Al-Mobarak, G. A. M. El-Sharkawy, and K. D. Warren, “The electronic spectra of the hexahalo anions of osmium(IV) and iridium(IV),” *Inorg. Chem.* **11**, 787 (1972).
- ⁴²B. Henderson and G. F. Imbusch, “Optical Spectroscopy of Inorganic Solids,” (Oxford University Press, 1989) pp. 274-6.
- ⁴³D. L. Dexter, “Absorption of Light by Atoms in Solids,” *Phys. Rev.* **101**, 48 (1956).
- ⁴⁴W. Beall Fowler, “Electronic States and Optical Transitions of Color Centers,” in *Physics of Color Centers* (edited by W. Beall Fowler, Academic Press, New York, 1968), Chap. 2, p. 72.
- ⁴⁵I. Bhaumik, R. Bhatt, S. Ganesamoorthy, A. Saxena, A. K. Karnal, P. K. Gupta, A. K. Sinha, and S. K. Deb, “Temperature-dependent index of refraction of monoclinic Ga₂O₃ single crystal,” *Appl. Opt.* **50**, 6006 (2011).
- ⁴⁶K. Saito, Y. Eishiro, Y. Nakao, H. Sato, and S. Sakaki, “Oscillator Strength of Symmetry-Forbidden d-d Absorption of Octahedral Transition Metal Complex: Theoretical Evaluation,” *Inorg. Chem.* **51**, 2785 (2012).

Table I. Parameters describing the g matrix of Ir^{4+} ions in $\beta\text{-Ga}_2\text{O}_3$ crystals. The g matrix is first given in the a, b, c^* coordinate system, and then in its diagonal form. Principal-axis directions are specified by a polar angle Θ and an azimuthal angle Φ . The polar angle Θ is defined relative to the c^* direction and the azimuthal angle Φ is defined relative to the a direction with positive rotation from a toward b in the c^* plane.

g matrix (in a, b, c^* coordinate system)			
	2.644	0	-0.195
		1.815	0
			0.559
principal values			
	g_{xx}	g_{yy}	g_{zz}
	2.662	1.815	0.541
principal directions			
	X	Y	Z
Θ	95.3°	90°	5.3°
Φ	0°	90°	0°
g matrix (principal values) for Ir^{4+} ions in rutile TiO_2 (from Ref. 30)			
	2.397	1.707	0.418

Table II. Correlation of the infrared absorption band and EPR signal from Ir^{4+} ions in $\beta\text{-Ga}_2\text{O}_3$ crystals. The Mg-doped crystals are labeled Mg1 and Mg2 and the Fe-doped crystals are labeled Fe1 and Fe2. Values are given for the thickness (i.e., optical path length), volume, absorption coefficient α of the infrared peak at room temperature for E along the a direction, and the concentration N obtained from the EPR signal.

sample	thickness (mm)	volume (mm^3)	absorption coefficient α (cm^{-1})	concentration from EPR N (10^{18} cm^{-3})	N/α (10^{18} cm^{-2})
Mg1	1.19	14.5	2.90	7.0	2.4
Mg2	1.41	12.0	2.77	6.0	2.2
Fe1	0.36	4.6	0.46	1.2	2.7
Fe2	0.38	4.2	0.43	1.0	2.3
average $N/\alpha = 2.4$					

Figure Captions

FIG. 1. EPR spectrum taken at 30 K from an Mg-doped β -Ga₂O₃ crystal. The magnetic field is along the b direction and the microwave frequency is 9.393 GHz. The Ir⁴⁺ line is at 369.9 mT. The other four sharper lines are from the $S = 5/2$ Fe³⁺ ions.

FIG. 2. Angular dependence of the Ir⁴⁺ EPR spectrum in a β -Ga₂O₃ crystal. Data were taken in the a - b , b - c , and c - a^* planes. The discrete points are experimental results, and the solid lines are computer-generated using the g values listed in Table I. Magnetic field values along the left vertical axis correspond to a microwave frequency of 9.401 GHz.

FIG. 3. Infrared absorption band from Ir⁴⁺ ions in an Mg-doped β -Ga₂O₃ crystal. Spectra were obtained at room temperature (blue curve) and at 80 K (red curve). Light propagated along the b direction with the electric field vector E along the a direction.

FIG. 4. Polarization dependence of the infrared absorption band from Ir⁴⁺ ions in an Mg-doped β -Ga₂O₃ crystal. These spectra were taken with the electric field E along the b direction (spectrum 1), the a direction (spectrum 2), and the c direction (spectrum 3). Light propagated along the c direction for spectrum 1 and the b direction for spectra 2 and 3.

FIG. 5. Intensity of the Ir⁴⁺ infrared absorption band in an Mg-doped β -Ga₂O₃ crystal when the direction of the electric field E is rotated from a to c^* in the crystal. The solid line represents a $\cos^2\theta$ dependence.

Fig. 6. EPR spectra from an Mg-doped β -Ga₂O₃ crystal taken at 40 K before and after an irradiation at 77 K with x rays. Identical spectrometer settings were used when acquiring the two spectra. (a) Before the irradiation, only the Fe³⁺ and Ir⁴⁺ signals are present. (b) After the irradiation, and with no warming step, the Mg_{Ga}⁰ signal is present and the Fe³⁺ and Ir⁴⁺ signals have decreased.

Fig. 7. EPR spectra from an Fe-doped β -Ga₂O₃ crystal taken at 40 K before and after an irradiation at 77 K with x rays. The upper left (Fe³⁺) and upper right (Ir⁴⁺) spectra were taken before the irradiation. The lower left (Fe³⁺) and lower right (Ir⁴⁺) spectra were taken after the irradiation. One set of spectrometer operating conditions was used for the two Fe³⁺ spectra and a different set was used for the two Ir⁴⁺ spectra. The two Fe³⁺ spectra can be directly compared and the two Ir⁴⁺ spectra can be directly compared.

ACCEPTED MANUSCRIPT

Figure 1

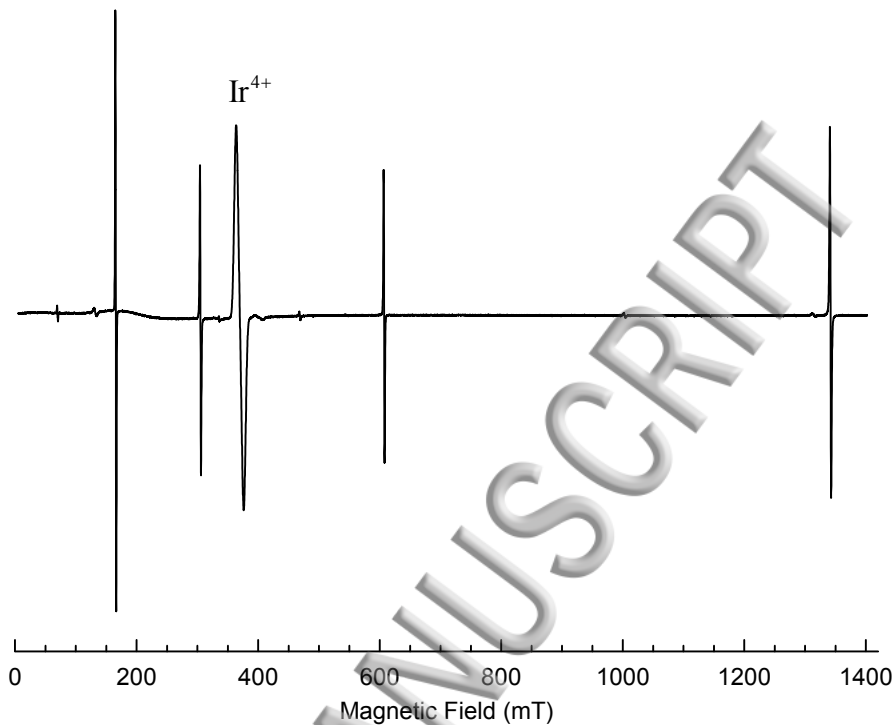


Figure 2

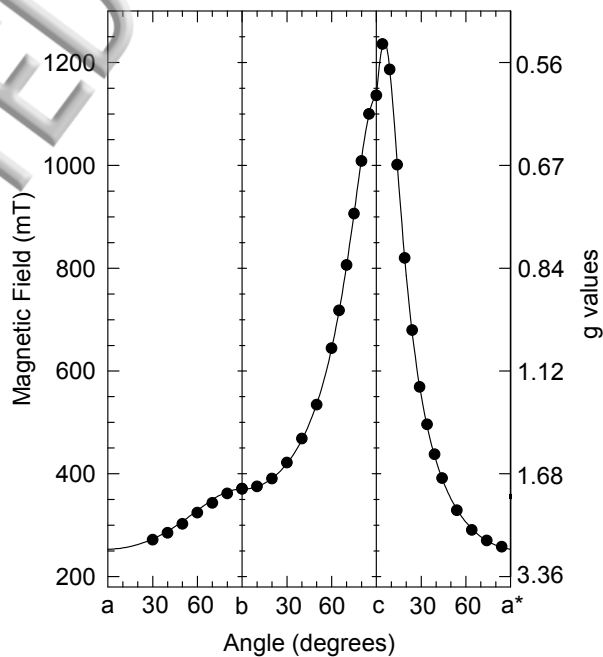


Figure 3

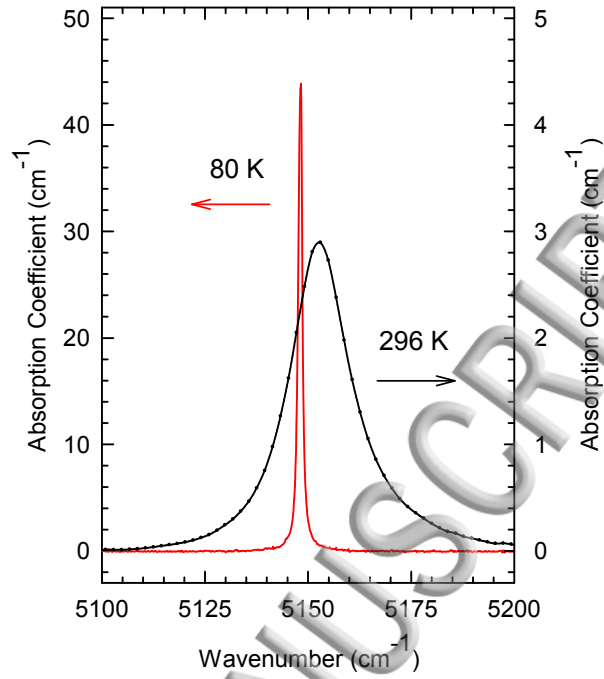


Figure 4

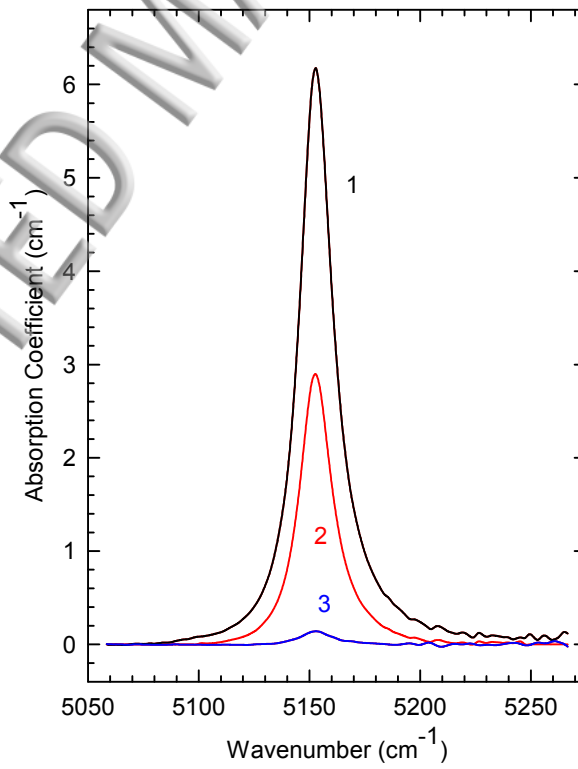


Figure 5

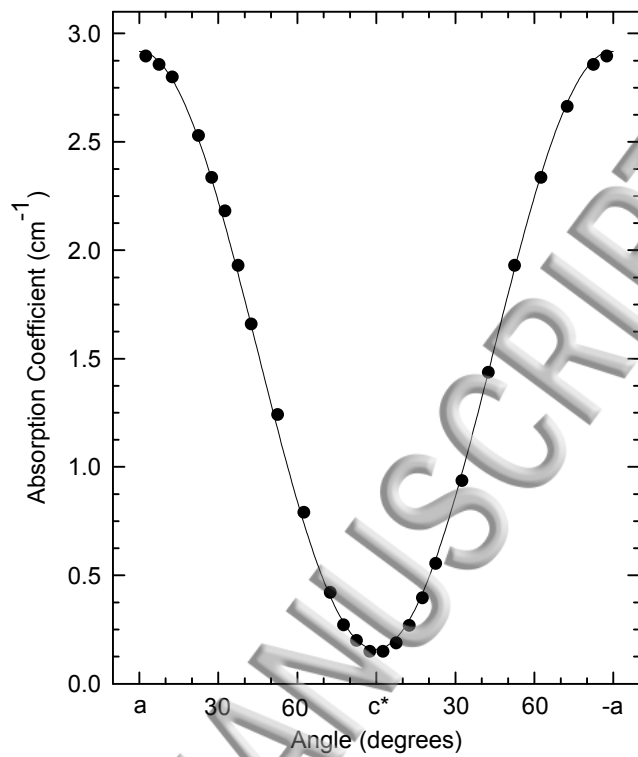


Figure 6

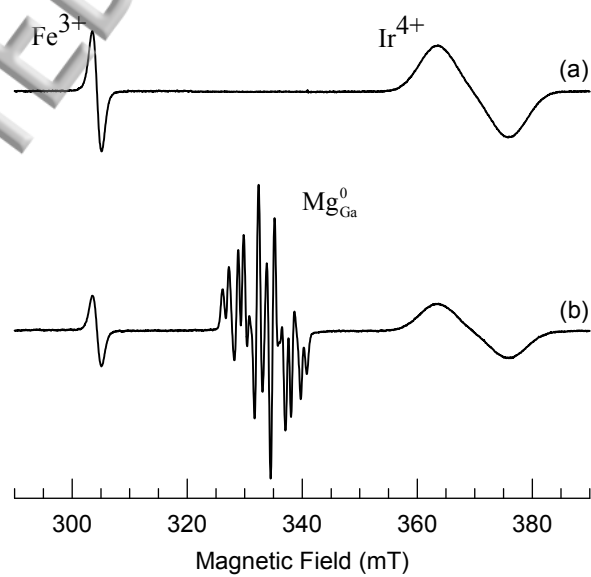
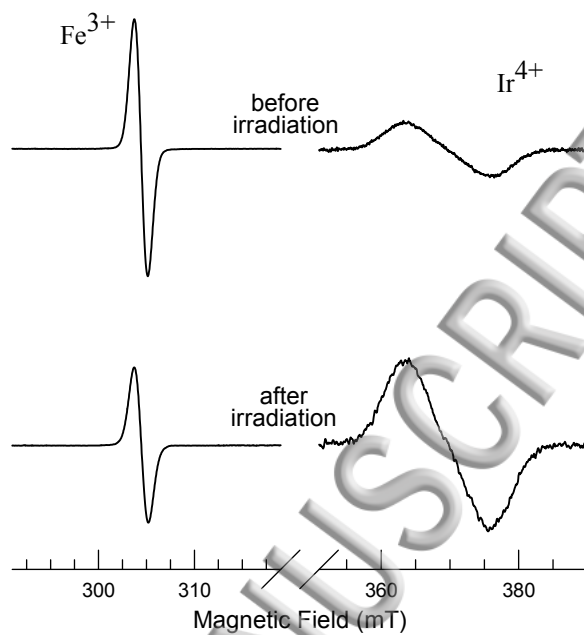
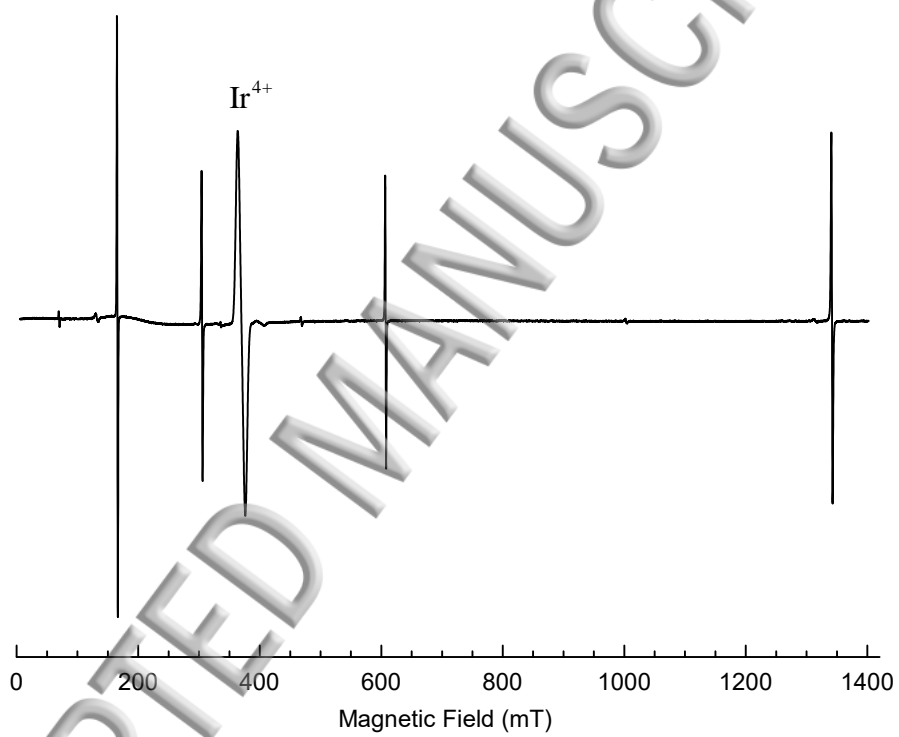
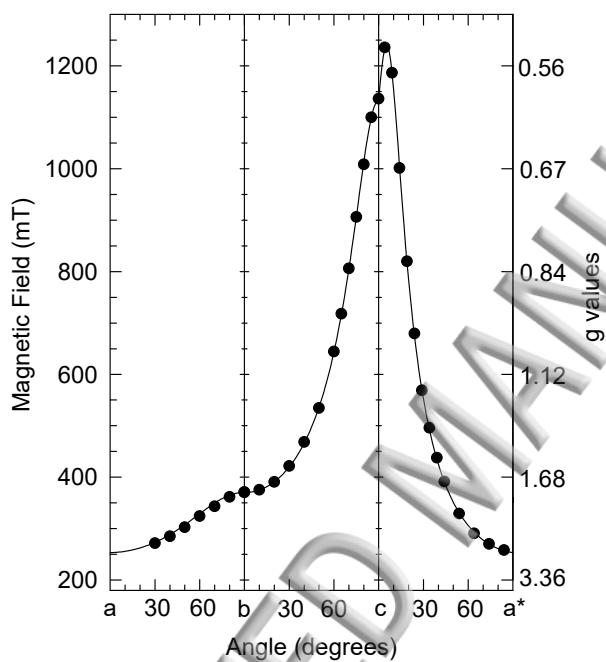


Figure 7







ACCEPTED MANUSCRIPT

